

**Staggered quantum walks with superconducting microwave resonators**

J. Khatibi Moqadam and M. C. de Oliveira

*Instituto de Física “Gleb Wataghin”, Universidade Estadual de Campinas, Campinas, SP, Brazil*

R. Portugal

*Laboratório Nacional de Computação Científica (LNCC), Petrópolis, RJ, Brazil*

(Received 3 October 2016; revised manuscript received 31 January 2017; published 5 April 2017)

The staggered quantum walk is a model defined by the product of local operators associated with two or more independent graph tessellations. This model is versatile, encompasses several well-known discrete-time quantum walks, and inherits interesting features of the continuous-time quantum walk. We propose an implementation of the staggered quantum walk model with superconducting microwave resonators, where the required local operations are provided by the nearest neighbor interaction of the resonators coupled through superconducting quantum interference devices. The tunability of the interactions makes this system an excellent toolbox for this class of quantum walks. We focus on the one-dimensional case and discuss its generalization to a more general class known as triangle-free graphs.

DOI: [10.1103/PhysRevB.95.144506](https://doi.org/10.1103/PhysRevB.95.144506)**I. INTRODUCTION**

Quantum walks are the quantum generalization of random walks, and form the building blocks in designing quantum search algorithms outperforming the similar classical ones [1]. The two main paradigms in this respect are the coined discrete-time quantum walk (DTQW) [2] and the continuous-time quantum walk (CTQW) [3]. In one-dimensional (1D) DTQWs, a two-level quantum system works as a coin, whose quantum property to exist in a superposition of states gives the distinct ballistic spreading of the walker encoded in a set of discrete states. In CTQWs, it is the excitation exchange between the neighboring sites, in a lattice, that directly works as a walker without the need of a coin. Typically a tight-binding Hamiltonian followed by a linear coupling between excitations in bosonic modes suffices to implement the CTQW model, making its implementation convenient (see Ref. [4] for an example with nanomechanical resonators). However, when the data structure is a lattice with dimension less than four, search algorithms based on the standard CTQW do not outperform the classical algorithms based on random walks [5].

Recently, a general class of coinless discrete-time quantum walks was proposed—the staggered quantum walk (SQW) [6–8], which includes the quantum walks studied in Refs. [9,10] as particular cases. This model also includes as particular cases the flip-flop coined DTQWs with Hadamard and Grover coins and the entire Szegedy’s quantum walk model [11]. In the language of graph theory, the required unitary operators (not Hamiltonians) can be obtained by a graphical method based on graph tessellations. A tessellation is a partition of the set of nodes into cliques; that is, each element of the partition is a clique. A clique is a subgraph that is complete, namely all nodes of a clique are neighbors.

We have proposed an extension of the SQW model, called SQW with Hamiltonians [12], which uses the graph tessellations to define local Hamiltonians instead of the local unitary evolution operators. The extended model includes the quantum walks analyzed in Ref. [13] as particular cases. The SQW with Hamiltonians is fitted for the implementation through bosonic nearest neighbor interactions, similarly to

the CTQW, with the advantage of being able to outperform classical search algorithms at lower dimensional lattice structures [14]. This advantage comes at a price, which is the necessity to implement time dependent (piecewise-constant) controlled evolution, requiring highly controllable systems for its implementation.

Superconducting quantum circuits supporting microwave photons are promising for realizing the required evolutions in quantum computation [15–17] and quantum simulation [18,19]. Besides the tunneling devices employed for qubit encoding, superconducting circuits allow the realization of lattices of coupled elements. Achieving tunable couplings between circuit elements is a crucial step. Tunable strong coupling among superconducting elements has been achieved in several ways, using both superconducting quantum interference devices (SQUIDs) and qubits [20–34]. Recently, structured arrays of microwave superconducting resonators with SQUID tunable couplings [20–22] have been investigated on dedicated simulations of many-body models with engineered interactions [35–39]. The evolution of those systems cannot be simulated with conventional static-coupling quantum simulators. Notwithstanding, those arrays could be employed for more general quantum tasks. Specially, an array of microwave resonators with switchable couplings can be directly employed for simulating the SQW dynamics.

In this work we propose the implementation of the SQW model on a system composed of microwave resonators coupled through SQUIDs. The implementation is analyzed in detail on a 1D lattice, which is used as a prototype to describe a more general dynamics on triangle-free graphs. In that class of graphs, which includes  $N$ -dimensional square lattices and trees, the resonators interact in a pairwise way in each element of the tessellation. The conventional optical and electron-beam lithography technologies that are used in fabricating superconducting-circuit-based devices allow us to construct a large scale lattice with an arbitrary geometry. The lattice dynamics can then be coherently controlled using external electromagnetic fields. Moreover, due to typically

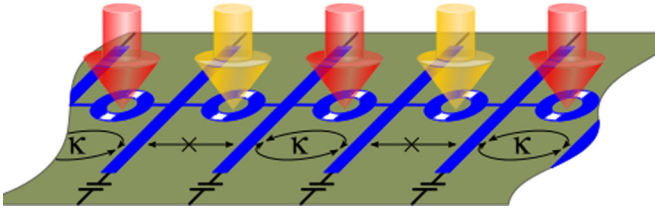


FIG. 1. Array of superconducting microwave resonators coupled through SQUID elements. Disjoint pairs of coupled resonators (with the coupling strength  $\kappa$ ) are realized by applying magnetic pulses with two different intensities, namely the strong (red/dark-gray) and the weak (yellow/light-gray) pulses on the SQUIDs. The SQW dynamics is implemented by alternating the application of pulses with a fixed period.

large coherent times in superconducting circuits, more walk steps can be realized in such systems than in any previous implementation [40].

The remainder of the paper is organized as follows. In Sec. II we present the Hamiltonian of the superconducting circuit employed to simulate the dynamics. In Sec. III we describe the dynamics of the staggered quantum walks on the line and show how it can be implemented with superconducting microwave resonators. In Sec. IV we discuss the generalization for triangle-free graphs and present our conclusions. The Appendixes describe a formal derivation of the Hamiltonian used in this work and the system parameters.

## II. SUPERCONDUCTING CIRCUIT

Let us consider a 1D array of coupled superconducting microwave resonators, as in Fig. 1, which can be made from finite sections of superconducting transmission line [18] or stripline [21,22]. The resonators couplings are mediated by SQUID elements. Each SQUID is controlled by an individual wave generator that produces magnetic flux pulses providing the system with tunable couplings (see the Appendixes for the formal derivation of the system dynamics). The Hamiltonian for the system is written as ( $\hbar = 1$ )

$$\mathcal{H} = \sum_n \omega_n a_n^\dagger a_n - \sum_{(n,m)} \kappa_{nm}(\Phi_{\text{ext}})(a_n^\dagger a_m + a_m^\dagger a_n), \quad (1)$$

where  $\omega_n$  are the resonators frequencies,  $a_n^\dagger$  and  $a_n$  are the creation and annihilation operators satisfying  $[a_n, a_m^\dagger] = \delta_{nm}$ , and  $\kappa_{nm}(\Phi_{\text{ext}})$  are the flux dependent couplings between adjacent ( $m = n \pm 1$ ) resonators. Hamiltonian (1) represents the tight-binding model with controllable hopping strengths  $\kappa_{nm}(\Phi_{\text{ext}})$ . Similar tunable coupling with SQUIDs has also been discussed in Refs. [20,37].

The SQUID coupler is specially appropriate, since it allows turning on and off the coupling between the two resonators, hence working as a switch. Actually, two different states, namely a given large coupling  $\kappa$  and no coupling, are required here. Such states can be implemented by applying two different pulses through the corresponding wave generator, say  $\Phi_{\text{on}}$  and  $\Phi_{\text{off}}$ , such that  $\kappa_{nm}(\Phi_{\text{on}}) = \kappa$  and  $\kappa_{nm}(\Phi_{\text{off}}) = 0$ . Such ability to switch on and off the couplings is essential for our model.

There are several methods to prepare the system in a predefined state of the resonators and also to measure their

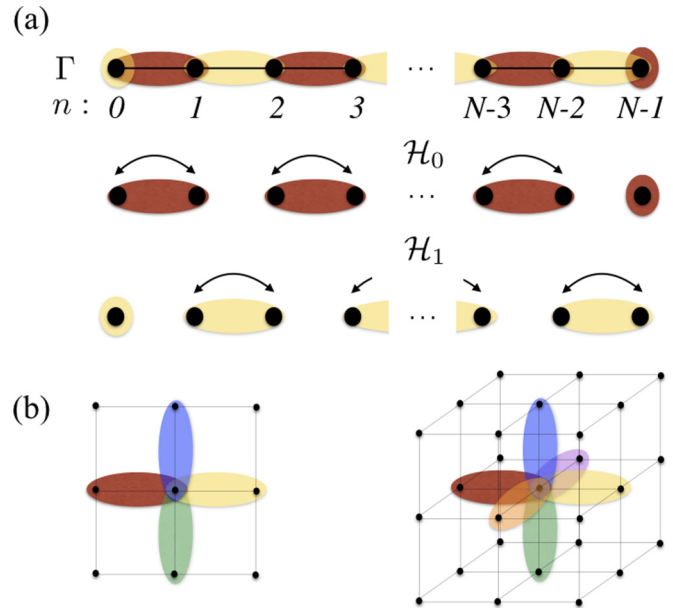


FIG. 2. (a) A 1D array, with the two possible tessellations, namely the red/dark-gray and the yellow/light-gray ovals. Each tessellation is a partition of the set of nodes into cliques (a clique is a subgraph in which every two distinct nodes are connected by an edge). Moreover, the set of edges are covered in the union of all tessellations. Each tessellation corresponds to a Hamiltonian. (b) The “unit cells” for the two- and three-dimensional lattices. For the  $N$ -dimensional lattice  $2N$  different tessellations are required.

state after the evolution. We are interested in describing a single-particle walker, therefore methods for single-photon generation and detection are required [41–43]. In order to prepare and measure photons in an arbitrary resonator, individual transmon qubits [44] are coupled capacitively to the resonators. Each transmon qubit is also coupled capacitively to a separate superconducting resonator—a coplanar waveguide cavity, which is required for manipulating the qubit state. The dynamics of the transmon qubit coupled to the  $n$ th resonator in near resonant regime is described by the Jaynes-Cummings Hamiltonian. The way those additional devices are employed for photon generation and detection is described after exploring the system dynamics.

## III. STAGGERED QUANTUM WALK DYNAMICS

A SQW on the 1D lattice is defined by two tessellations described in Fig. 2(a). The set of  $N$  nodes of the array can be associated with the canonical basis  $\{|n\rangle : n = 0 \dots N-1\}$ , where  $|n\rangle$  is a  $N$ -component unit vector with 1 in the  $(n+1)$ th entry and 0 otherwise, spanning the  $N$ -dimensional Hilbert space. We associate vectors  $|\alpha_n\rangle = (|n\rangle + |n+1\rangle)/\sqrt{2}$  with the 2-node elements (colored ovals in Fig. 2) of both tessellations and  $|\alpha_{N-1}\rangle = |N-1\rangle$ ,  $|\alpha_N\rangle = |0\rangle$  with the 1-node elements. Even (odd)  $n$  refers to red (yellow) tessellation. The Hamiltonian for the red (yellow) tessellation is

$$\mathcal{H}_{0(1)} = 2 \sum_{\substack{n \text{ even} \\ (n \text{ odd})}} |\alpha_n\rangle \langle \alpha_n| - \mathcal{I}_N, \quad (2)$$

where  $\mathcal{I}_N$  is the  $N$ -dimensional Hilbert space identity operator [12]. The Hamiltonians are block diagonal, and each block is given by the Pauli matrix  $\sigma_x$ . The local operator of SQW is defined as  $\mathcal{U}_{0(1)} = \exp(i\theta\mathcal{H}_{0(1)})$ , where  $\theta$  is an angle [12]. Since the Hamiltonians are block diagonal, the operators are diagonal as well and the blocks are given by  $\exp(i\theta\sigma_x)$ . The SQW dynamics is driven by successive applications of  $\mathcal{U}_1\mathcal{U}_0$ , starting from an initial state.

The SQW dynamics can be achieved by controlling the superconducting circuit. We consider Hamiltonian (1) in the single-photon regime  $\sum_n \langle a_n^\dagger a_n \rangle = 1$ . Therefore the state of the system with  $N$  resonators belongs to the  $N$ -dimensional Hilbert space, which is given in terms of the canonical basis  $\{|n\rangle\}$  previously described. The resonators are considered in resonance at frequency  $\omega$ . For the required dynamics, the Hamiltonians  $\mathcal{H}_0$  and  $\mathcal{H}_1$  in Eq. (2) are slightly modified by substituting  $\sigma_x$  with  $\omega\mathcal{I}_2 - \kappa\sigma_x$ . The modified Hamiltonians for  $N$  odd [45] can be written in the explicit form

$$\mathcal{H}_0 = \begin{bmatrix} \mathcal{I}_{(N-1)/2} \otimes (\omega\mathcal{I}_2 - \kappa\sigma_x) & \mathbf{0} \\ \mathbf{0} & \omega \end{bmatrix} \quad (3)$$

and

$$\mathcal{H}_1 = \begin{bmatrix} \omega & \mathbf{0} \\ \mathbf{0} & \mathcal{I}_{(N-1)/2} \otimes (\omega\mathcal{I}_2 - \kappa\sigma_x) \end{bmatrix}. \quad (4)$$

Noncommuting Hamiltonians  $\mathcal{H}_0$  and  $\mathcal{H}_1$  are referred to as even and odd, respectively. Here we explicitly consider open boundary conditions, and with a small modification periodic boundary conditions could also be addressed. Since we simulate the dynamics far from the boundaries, corresponding to the walk on the line, this choice is not relevant.

The even (odd) Hamiltonian is constructed by switching on only the couplings  $\kappa_{n,n+1}$  with even (odd) index  $n$ , directly corresponding to the tessellation in Fig. 2(a). We are interested in controlling the system by alternating between the even and the odd Hamiltonians, in certain time steps  $\tau$ . Therefore, we apply the flux pulses  $\Phi_{\text{on}}$  and  $\Phi_{\text{off}}$  (see the Appendixes), such that in the time interval  $[0, 2\tau)$  the couplings assume the form

$$\begin{aligned} \kappa_{nm}(\Phi_{\text{ext}}) &= \kappa, \\ \kappa_{np}(\Phi_{\text{ext}}) &= \kappa_{qm}(\Phi_{\text{ext}}) = 0, \quad \forall (p, q) \neq (m, n), \end{aligned} \quad (5)$$

where  $n = 2\ell$  for  $t \in [0, \tau)$ , and  $n = 2\ell + 1$  for  $t \in [\tau, 2\tau)$ , in which  $\ell = 0 \cdots (N-1)/2$  (note that  $m = n \pm 1$  for the 1D array). The system setup during  $[0, \tau)$  is given in Fig. 1, where the red (yellow) magnetic pulses associated with the flux  $\Phi_{\text{on}}$  ( $\Phi_{\text{off}}$ ). In  $[\tau, 2\tau)$ , the magnetic pulses are interchanged. The realization of such time dependent couplings implies that the system is described by the Hamiltonian

$$\mathcal{H}(t) = \begin{cases} \mathcal{H}_0, & t \in [0, \tau), \\ \mathcal{H}_1, & t \in [\tau, 2\tau), \end{cases} \quad (6)$$

which generates the evolution operator

$$\mathcal{U}(2\tau) = \mathcal{U}_1(\tau) \mathcal{U}_0(\tau), \quad (7)$$

where  $\mathcal{U}_0$  ( $\mathcal{U}_1$ ) corresponds to the evolution of the time-independent Hamiltonian  $\mathcal{H}_0$  ( $\mathcal{H}_1$ ).  $\mathcal{U}_0$  ( $\mathcal{U}_1$ ) is easily calculated from the exponential of the  $2 \times 2$  matrices in the block

diagonal Hamiltonian  $\mathcal{H}_0$  ( $\mathcal{H}_1$ ),

$$e^{-i\tau(\omega\mathcal{I}_2 - \kappa\sigma_x)} = e^{-i\omega\tau} \begin{bmatrix} \cos \kappa\tau & i \sin \kappa\tau \\ i \sin \kappa\tau & \cos \kappa\tau \end{bmatrix}. \quad (8)$$

The parameter  $\theta$  introduced in the mathematical model is now set as  $\theta = \kappa\tau$ , by adjusting the time interval  $\tau$ , and as far as the resonators are in resonance, the role of  $e^{-i\omega\tau}$  in (8) is irrelevant. This procedure allows us to implement a general 1D-SQW dynamics. For instance, by setting  $\kappa\tau = 2\pi\ell + \pi/4$ , for an integer  $\ell$ , the blocks of the evolution operators  $\mathcal{U}_0$  and  $\mathcal{U}_1$  take the form of the Hadamard-like operator

$$H = \frac{1}{\sqrt{2}} \begin{bmatrix} 1 & i \\ i & 1 \end{bmatrix}, \quad (9)$$

and the quantum walk model introduced in Ref. [13] is recovered. To have the fastest spread of the walker's probability distribution one must set  $\kappa\tau = 2\pi\ell + \pi/3$  [12].

In the following, we consider the time evolution of the system for the period  $t = 2\tau l$  with  $l$  an integer number, under the repeated application of operator (7), leading to  $[\mathcal{U}(2\tau)]^l$ . The evolution starts with the initial state

$$|\psi_0\rangle = |(N-1)/2\rangle, \quad (10)$$

representing a single photon in resonator  $(N-1)/2$ , the middle resonator of the chain. In order to produce such initial state, first all the couplings are turned off, and then a single photon is generated in resonator  $(N-1)/2$ . Generating a single photon in a resonator of the system is possible by promoting the corresponding transmon to its first excited state and then mapping the excitation into the resonator. The protocol begins by exciting the transmon by applying a  $\pi$  pulse through the coplanar waveguide (CPW) cavity, while the qubit is detuned from the system resonator (CPW cavity and system resonator must have different different frequencies). Then the transmon is brought to resonance with the system resonator for the time  $t_{\text{Rabi}} = \pi/2\lambda$  ( $\lambda$  is the qubit-resonator coupling strength) to transfer its excitation to the resonator.

Now the system evolves as

$$|\psi_l\rangle = [\mathcal{U}(2\tau)]^l |\psi_0\rangle, \quad (11)$$

for a given integer  $l$ . At this stage, we measure the system by detecting all the resonators. That can be done by turning off all the couplings, and then measuring the population of all the resonators. A resonator photon number detection is processed by bringing the transmon into resonance with the resonator for  $t_{\text{Rabi}} = \pi/2\lambda$ , hence the (excited) resonator transfer back the photon to the qubit. Spectroscopy of the transmon transition frequency through far detuned CPW cavity then gives the information about the photon number in the resonator. Such measurement protocol, however, destroys the photon in the system resonator. To have a nondemolition measurement of the photon number, the transmon should interact with the system resonator in a quasidispersive regime [41]. In this case, the transition frequency of the transmon is stark shifted depending on the number of photons, 0 or 1, in the system resonator. Now the spectroscopy of the transmon transition frequency gives information about the photon number in the system resonator, in a nondemolition way.

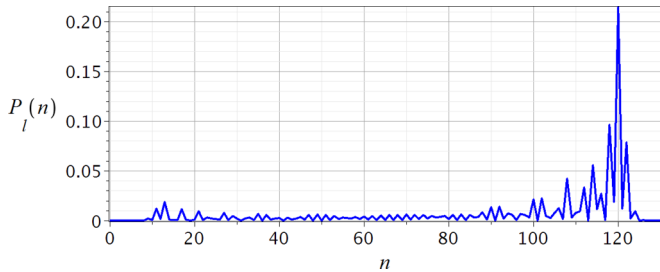


FIG. 3. Photon probability distribution for a linear array of  $N = 133$  resonators after  $l = 32$  steps ( $t = 64\tau$ ). The photon is initially generated in the middle resonator of the array and  $\kappa\tau$  is tuned for maximum spread.

Whatever the method employed, the probability distribution of finding the photon in the array is computed to give

$$P_l(n) = |\langle n | \psi_l \rangle|^2, \quad (12)$$

for  $n = 0 \cdots N - 1$ . Figure 3 shows the photon probability distribution for a linear array of  $N = 133$  resonators after  $l = 32$  steps ( $t = 64\tau$ ), when  $\kappa\tau = 2\pi l + \pi/3$  (maximum spread). The dynamics of the photon probability distribution is ballistic—a clear signature of the quantum walk. It should be mentioned that for obtaining the probability distribution in Fig. 3 the above process of initialization, evolution, and measurement should be repeated many times. However, due to the ballistic evolution of the quantum walk, the major part of the probability distribution is concentrated around a few resonators far from the initial position. Knowing that the measurement stage can be performed on a considerably smaller number of resonators.

#### IV. FINAL CONSIDERATIONS

To conclude we discuss the extension of the described 1D implementation to a class of graphs called triangle-free graphs, which includes  $N$ -dimensional lattices, trees, and many other topologies. A graph is triangle-free if no three nodes form a triangle of edges. To tessellate such a graph we make a partition of the node set by circling two neighboring nodes at a time. Two different circles cannot have a node in common and no node can be missed at the end of the process (there is the possibility of ending up with isolated single nodes that form singletons of the partition). The red partition in Fig. 2(a) is an example of this procedure. The circles are labeled then by  $\alpha_k$  for  $0 \leq k < c_0$ , where  $c_0$  is the number of circles in the partition. Having related a Hilbert space basis to the node set, we associate the unit vector  $|\alpha_k\rangle = (|i\rangle + |j\rangle)/\sqrt{2}$  with circle  $\alpha_k$  that contains the nodes  $i$  and  $j$  (if  $\alpha_k$  contains only node  $i$  then  $|\alpha_k\rangle = |i\rangle$ ). Accordingly, the Hamiltonian

$$\mathcal{H}_0 = 2 \sum_{k=0}^{c_0-1} |\alpha_k\rangle\langle\alpha_k| - \mathcal{I}_N \quad (13)$$

is defined for the tessellation associated with  $\{|\alpha_k\rangle\}$ . The vectors  $|\alpha_k\rangle$  have at most two nonzero entries in the computational basis and Hamiltonian  $\mathcal{H}_0$  is a reflection operator [12]. The same procedure is repeated to obtain a second tessellation, but the new partition must aim the edges that were not included in

the circles of the first partition. The new Hamiltonian  $\mathcal{H}_1$  can be obtained from Eq. (13) after replacing  $|\alpha_k\rangle$  with the vectors associated with the second partition and replacing  $c_0$  with  $c_1$ , where  $c_1$  is the number of circles in the second partition. The process is continued until all edges have been covered with circles and the Hamiltonian  $\mathcal{H}_{d-1}$  has been obtained. Besides, each node must be inside the intersection of  $d$  circles. This situation can be seen for dimensions higher than 1 in the “unit cells” in Fig. 2(b).

The evolution operator of a SQW with Hamiltonians in the class of triangle-free graphs has the form

$$\mathcal{U} = e^{i\theta\mathcal{H}_{d-1}} \cdots e^{i\theta\mathcal{H}_1} e^{i\theta\mathcal{H}_0}, \quad (14)$$

where  $\theta$  is an angle and  $d$  is the maximum vertex degree, that is, the maximum number of edges incident on a node. For  $N$ -dimensional lattices  $d = 2N$ , that can be verified for  $N = 2, 3$  in Fig. 2(b).

According to our prescription any desired triangle-free graph can be implemented using resonators and SQUIDs associated with the nodes and the edges of the graph, respectively. The system is described by Hamiltonian (1), where the first sum runs over all nodes and the second sum runs over all edges. Each of the Hamiltonians  $\mathcal{H}_0, \dots, \mathcal{H}_{d-1}$  can be implemented during the time period  $\tau$  by applying an appropriate set of magnetic pulses, such that the couplings take the form of Eq. (5), in which  $m, n$  belong to a suitable  $\alpha_k$ . The corresponding setup of the system, in each case, consists of a collection of disjoint pairs of coupled resonators, similar to the setup in Fig. 1. Therefore, the time-independent Hamiltonians can be implemented during the time interval  $[0, \tau d]$  leading to the evolution (14). We remark that quantum search algorithms [6] employing the present proposal can be readily implemented. For that an extra local Hamiltonian associated with a nonhomogeneous tessellation is required.

Although restricted to implement the single-photon staggered quantum walk model, the system proposed in this paper is quite general and can be employed to simulate multiparticle quantum dynamics, in particular, it can realize boson sampling [46]. While single photons can be loaded in various resonators there is no need to measure more than one photon in each resonator because that is a rare event in the boson sampling protocol. Actually, tunable couplings between the resonators enable our system to implement microwave boson sampling, and in this respect our system is similar to the system presented in Ref. [47]. However, besides the possibility of realizing the boson sampling problem, we have addressed specially the implementation of the search problem in the system (see Ref. [46] for discussions regarding search problem in a boson computer). It should be noted that the sampling problem requires unitary operators that are randomly chosen according to the Haar measure [46]. In contrast, the quantum dynamics considered here corresponds to structured unitary operators, which are easy for boson sampling problem. In this way, the staggered quantum walk is not strictly equivalent to single-photon boson sampling.

Finally, considering that the coupling strength is about 10 MHz (see the Appendixes) and the single photon lifetime in the resonators is around 100  $\mu\text{s}$  or higher [15], there is enough time to realize a considerable number of steps. Moreover, the magnetic pulses should be switched within 0.1  $\mu\text{s}$ .



Imperfection in the resonators and couplings frequencies can affect the dynamics producing, for example, wave function localization. However, it is expected that the system can tolerate small imperfections in the couplings similarly to the continuous-time dynamics [4].

### ACKNOWLEDGMENTS

J.K.M. acknowledges financial support from CNPq Grant PDJ 165941/2014-6. M.C.O. acknowledges support by FAPESP through the Research Center in Optics and Photonics (CePOF) and by CNPq. R.P. acknowledges financial support from Faperj (Grant No. E-26/102.350/2013) and CNPq (Grants No. 303406/2015-1 and No. 474143/2013-9).

### APPENDIX A: DERIVATION OF THE SYSTEM HAMILTONIAN

Here we derive formally Hamiltonian (1) corresponding to the circuit in Fig. 1 in the main text, which follows by quantizing the classical Lagrangian of the circuit.

Consider a one-dimensional array of coupled superconducting microwave resonators, as in Fig. 4(a). The microwave resonator, here a transmission line resonator, can be considered as a two-wire line, each piece of infinitesimal length of which can be modeled as a  $LC$  circuit, with the inductance and capacitance per unit length  $l$  and  $c$ , respectively as shown in Fig. 4(b) [48]. Considering the flux variable  $\psi_n(x,t)$  along the transmission line resonator, the corresponding Lagrangian is given by [49]

$$\mathcal{L}_n^R = \int_{-L}^L \left[ \frac{c}{2} (\partial_t \psi_n)^2 - \frac{1}{2l} (\partial_x \psi_n)^2 \right] dx, \quad (\text{A1})$$

where  $c$  and  $l$  are considered position independent and, without loss of generality, supposed to be identical for all the resonators.

For a symmetrical SQUID, consisting of a superconducting ring interrupted by two identical Josephson junctions, the Lagrangian is written as

$$\mathcal{L}_n^S = \frac{1}{2} C_J (\dot{\phi}_{n,1}^2 + \dot{\phi}_{n,2}^2) + E_J (\cos \varphi_{n,1} + \cos \varphi_{n,2}), \quad (\text{A2})$$

where  $C_J$  is the junction capacitance,  $E_J$  is the Josephson energy, and  $\varphi_{n,1(2)}$  and  $\phi_{n,1(2)}$  are the flux and the phase differences across the junctions, respectively. The flux and the phase differences are related by  $\varphi_{n,1(2)} = 2\pi \phi_{n,1(2)} / \Phi_0$ , where  $\Phi_0$  is the flux quantum. Again, without loss of generality, all the SQUIDS are assumed to have the same  $C_J$  and  $E_J$ .

The fluxoid quantization along the SQUID loop is given by  $\phi_{n,1} + \phi_{n,2} + \Phi_{\text{tot},n} = k\Phi_0$ , where  $\Phi_{\text{tot},n}$  is the total flux enclosed by the loop and  $k$  is an integer number [50]. The total flux is the sum of the externally applied flux  $\Phi_{\text{ext},n}$ , subjecting the SQUIDS individually, and the flux generated by the currents circulating through the loop. Here it is assumed that the flux produced by the circulating currents is negligible hence  $\Phi_{\text{tot},n} \approx \Phi_{\text{ext},n}$ . In this case, for the symmetrical SQUID, it is possible to write  $(\phi_{n,1} - \phi_{n,2})/2 = \psi_n(0,t) - \psi_{n+1}(0,t)$ . Now, the SQUID variables in Eq. (A2) can be eliminated by expressing the Lagrangian in terms of  $(\phi_{n,1} \pm \phi_{n,2})/2$ .

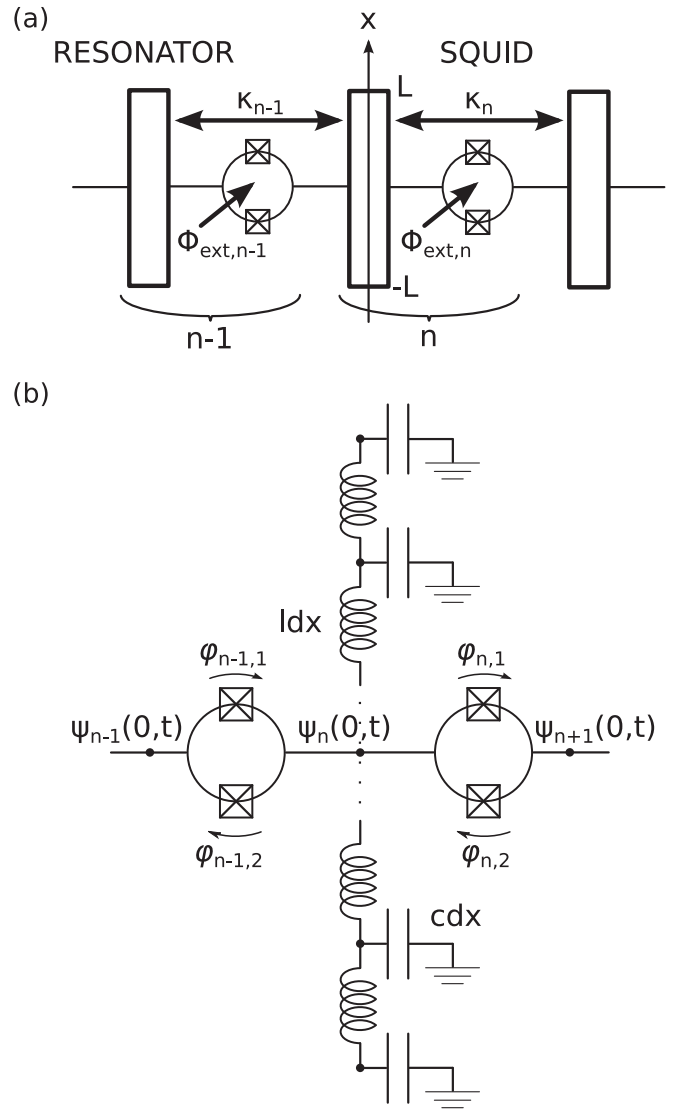


FIG. 4. Schematic representation of the system in (a) and the system parameters with the lumped element model of the resonator in (b).

Specifically, the second term in Eq. (A2) changes to

$$2E_J \cos \left( \pi \frac{\Phi_{\text{ext},n}}{\Phi_0} \right) \cos \frac{2\pi}{\Phi_0} [\psi_n(0,t) - \psi_{n+1}(0,t)],$$

supposing  $k$  is an even integer. The flux-dependent cosine function can be expanded in terms of its argument  $(2\pi/\Phi_0)[\psi_n(0,t) - \psi_{n+1}(0,t)]$  and only the first terms be kept, when the argument is small. The small values for the argument correspond to small flux difference in the adjacent resonators. In the quantum regime, as discussed in the following, the argument is given in terms of the creation and annihilation operators of the adjacent resonators [see Eqs. (A18) and (A25)] which is small for low photon numbers in the system. In this case, it is sufficient to consider the expansion up to the second order terms and dismiss the higher order terms that correspond to nonlinear photon interactions [20]. Therefore, the SQUID

Lagrangian can be written as

$$\mathcal{L}_n^S = C_J [\partial_t \psi_n(0,t) - \partial_t \psi_{n+1}(0,t)]^2 - E_n(\Phi_{\text{ext}}) [\psi_n(0,t) - \psi_{n+1}(0,t)]^2, \quad (\text{A3})$$

where

$$E_n(\Phi_{\text{ext}}) = \frac{4\pi^2}{\Phi_0^2} E_J \cos \pi \frac{\Phi_{\text{ext},n}}{\Phi_0}, \quad (\text{A4})$$

implying each SQUID can be controlled individually using the individual external magnetic fields. Note that in Lagrangian (A3) all the terms independent of the flux variables have been disregarded.

The system can be described by the Lagrangian

$$\mathcal{L} = \sum_n \tilde{\mathcal{L}}_n^R + \mathcal{L}_n^I, \quad (\text{A5})$$

where, for each index  $n$ , the resonator Lagrangian  $\mathcal{L}_n^R$  and SQUID Lagrangians  $\mathcal{L}_{n-1}^S$  and  $\mathcal{L}_n^S$  are considered. The modified resonator Lagrangian is given by

$$\tilde{\mathcal{L}}_n^R = \mathcal{L}_n^R + 2C_J [\partial_t \psi_n(0,t)]^2 - (E_{n-1} + E_n) [\psi_n(0,t)]^2, \quad (\text{A6})$$

that includes all the terms containing  $\psi_n$ , hence, the terms corresponding to  $\psi_{n\pm 1}$  are left for  $\tilde{\mathcal{L}}_{n\pm 1}^R$ . The interaction Lagrangian

$$\mathcal{L}_n^I = -2C_J \partial_t \psi_n(0,t) \partial_t \psi_{n+1}(0,t) + 2E_n \psi_n(0,t) \psi_{n+1}(0,t) \quad (\text{A7})$$

includes the contributions that couple indices  $n$  and  $n+1$ , hence, those that couple indices  $n$  and  $n-1$  are left for  $\mathcal{L}_{n-1}^I$ .

Supposing the interaction energy between the adjacent resonators is small with respect to the energy of each resonator, the problem can be treated perturbatively. In this way, the equation of motion is derived without considering the interaction Lagrangian but then the corresponding solutions are used in the total Lagrangian that includes the interaction term. The Euler-Lagrange equation for the modified Lagrangian  $\tilde{\mathcal{L}}_n^R$  turns out to be

$$\int_{-L}^L (c \partial_t^2 \psi_n - l^{-1} \partial_x^2 \psi_n) dx + 4C_J \partial_t^2 \psi_n(0,t) + 2(E_{n-1} + E_n) \psi_n(0,t) = 0. \quad (\text{A8})$$

Away from the center of the resonator ( $x=0$ ), Eq. (A8) gives the wave equation  $\partial_t^2 \psi_n = (1/\sqrt{lc})^2 \partial_x^2 \psi_n$ , in which  $1/\sqrt{lc}$  is the velocity of the electromagnetic wave in the resonator. By letting  $\psi_n(x,t) = \xi_n(t) u_n(x)$  in the wave equation, the Sturm-Liouville equation

$$\frac{d^2}{dx^2} u_n = -k_n^2 u_n, \quad (\text{A9})$$

for the spatial mode is obtained. The equation corresponds to the  $n$ th resonator in which  $k_n = (\omega_n \sqrt{lc})$  is the wave number and  $\omega_n$  is the wave angular frequency. At  $x=0$ , Eq. (A8) gives

$$\left( \frac{du_n}{dx} \right)_{x=0^+} - \left( \frac{du_n}{dx} \right)_{x=0^-} = h_0 u_n(0), \quad (\text{A10})$$

which implies a discontinuity in the current passing through the resonator at  $x=0$ . Moreover,

$$h_0 = 2(-2C_J \omega_n^2 + E_{n-1} + E_n) l = -8\chi_c k_n^2 L + \frac{\chi_{l_{n-1}} + \chi_{l_n}}{L} \quad (\text{A11})$$

in which the dimensionless parameters

$$\chi_c = C_J (2Lc)^{-1}, \quad \chi_{l_n} = E_n (2Ll) \quad (\text{A12})$$

are the relative capacitance and the relative inverse inductance of the Josephson junctions with respect to the total resonator capacitance  $2Lc$  and total resonator inductance  $2Ll$ . Finally, at  $x = \pm L$  we impose the open boundary condition (zero current)

$$\left( \frac{du_n}{dx} \right)_{x=-L} = \left( \frac{du_n}{dx} \right)_{x=L} = 0. \quad (\text{A13})$$

The eigenfunctions of Eq. (A9) subjected to the constraints (A10) and (A13) can be written as

$$u_{n,v}(x) = \begin{cases} A_{n,v} \cos k_{n,v} x - B_{n,v} \sin k_{n,v} x, & -L \leq x \leq 0, \\ A_{n,v} \cos k_{n,v} x + B_{n,v} \sin k_{n,v} x, & 0 \leq x \leq L, \end{cases} \quad (\text{A14})$$

where the wave numbers  $k_{n,v}$  are the solutions of the transcendental equation

$$\tan k_{n,v} L = \frac{h_0}{2k_{n,v}} = -4\chi_c k_{n,v} L + \frac{\chi_{l_{n-1}} + \chi_{l_n}}{2k_{n,v} L}, \quad (\text{A15})$$

and the integer  $v$  labels different modes of oscillation. Note that one of the coefficients in Eq. (A14) is already known in terms of the other one, say  $B_{n,v} = h_0 A_{n,v} / 2k_{n,v}$ .

The eigenfunctions (A14), for a given resonator, form an orthogonal set for different modes  $v$  according to

$$\frac{1}{2} c \int_{-L}^L u_{n,v}(x) u_{n,v'}(x) dx + 2C_J u_{n,v}(0) u_{n,v'}(0) = \frac{1}{2} L c \delta_{v,v'}, \quad (\text{A16})$$

which also determines the value of  $A_{n,v}$ . Moreover, the derivatives of the eigenfunctions (A14), obey the relation

$$\frac{1}{2l} \int_0^L \frac{d}{dx} u_{n,v} \frac{d}{dx} u_{n,v'} dx + (E_{n-1} + E_n) u_{n,v}(0) u_{n,v'}(0) = \frac{1}{2} L c \omega_{n,v}^2 \delta_{v,v'}. \quad (\text{A17})$$

Figure 5(a) shows the graphical solutions for Eq. (A15) for some typical values of  $\chi_c$  and  $\chi_l$ . The first normal mode and its derivative which is proportional to the current are sketched in Fig. 5(b). The frequency of the first normal mode corresponds to the smallest positive solution of Eq. (A15). The discontinuity in the current is given by Eq. (A10) associating with the current flowing to the adjacent resonator.

The general solution for Eq. (A8) is obtained by summing over all normal modes  $\xi_{n,v}(t) u_{n,v}(x)$ , namely

$$\psi_n(x,t) = \sum_v \xi_{n,v}(t) u_{n,v}(x), \quad (\text{A18})$$

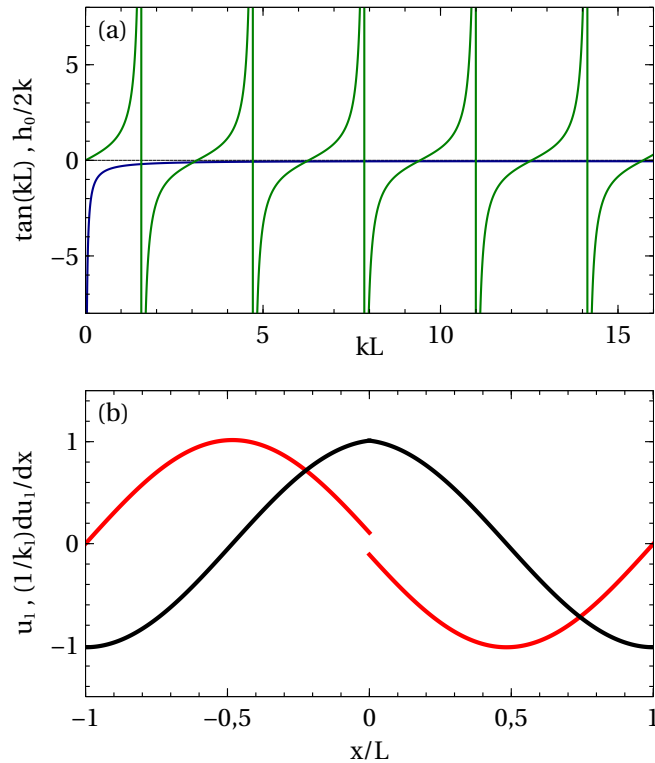


FIG. 5. Graphical solutions for Eq. (A15) with  $\chi_c = 0.5 \times 10^{-3}$  and  $\chi_{l_{n-1}} = \chi_{l_n} = -0.3059$  in (a), and the first normal mode and its derivative (the current) in (b) (the plot with the discontinuity at  $x = 0$  corresponds to the current). The frequency of the first normal mode is calculated as  $k_{n,1}L = 3.0351$ .

where each  $\xi_{n,v}(t)$  is the temporal part of the wave function corresponding to the mode  $v$ . Substituting the general solution (A18) in the modified resonator Lagrangian in Eq. (A6), and using the relations (A16) and (A17), we find

$$\tilde{\mathcal{L}}_n^R = \frac{1}{2}Lc \sum_v \dot{\xi}_{n,v}^2 - \omega_{n,v}^2 \xi_{n,v}^2, \quad (\text{A19})$$

which shows each (temporal) normal mode corresponds to an independent simple harmonic oscillator. Considering the modes  $\xi_{n,v}(t)$  as coordinates, the momentum conjugate to which are defined as

$$q_{n,v}(t) = \partial \tilde{\mathcal{L}}_n^R / \partial \dot{\xi}_{n,v} = Lc \dot{\xi}_{n,v}, \quad (\text{A20})$$

which can be used to write Hamiltonian (A19) as

$$\tilde{\mathcal{H}}_n^R = \frac{1}{2} \sum_v \frac{1}{Lc} q_{n,v}^2 + Lc \omega_{n,v}^2 \xi_{n,v}^2. \quad (\text{A21})$$

Moreover, substituting the general solution (A18) in the interaction Lagrangian (A7) and using the conjugate momentums (A20) gives

$$\mathcal{H}_n^I = \sum_v g_n^{\text{cap}} q_{n,v} q_{n+1,v} + g_n^{\text{ind}} \xi_{n,v} \xi_{n+1,v}, \quad (\text{A22})$$

where

$$g_n^{\text{cap}} = -\frac{2C_J}{(Lc)^2} u_{n,v}(0) u_{n+1,v}(0), \quad (\text{A23})$$

$$g_n^{\text{ind}} = 2E_n u_{n,v}(0) u_{n+1,v}(0), \quad (\text{A24})$$

and we have neglected the terms that couple any pair of different modes in the adjacent resonators.

Hamiltonians (A21) and (A22) can be quantized by introducing the creation and annihilation operators  $a_{n,v}^\dagger$  and  $a_{n,v}$ , respectively, corresponding to the excitations in mode  $v$  in resonator  $n$ . The operators obey the commutation relations  $[a_{n,v}, a_{m,v'}^\dagger] = \delta_{nm} \delta_{v,v'}$ . The coordinates  $\xi_{n,v}$  and the momentums  $q_{n,v}$  are then expressed as [49]

$$\hat{\xi}_{n,v} = \sqrt{\frac{\hbar}{2Lc\omega_{n,v}}} (a_{n,v} + a_{n,v}^\dagger), \quad (\text{A25})$$

$$\hat{q}_{n,v} = -i \sqrt{\frac{\hbar Lc\omega_{n,v}}{2}} (a_{n,v} - a_{n,v}^\dagger), \quad (\text{A26})$$

that turn Eq. (A21) into

$$\tilde{\mathcal{H}}_n^R = \sum_v \hbar \omega_{n,v} \left( a_{n,v}^\dagger a_{n,v} + \frac{1}{2} \right), \quad (\text{A27})$$

which is the quantized harmonic oscillator Hamiltonian with infinite noninteracting modes. However, we restrict the harmonic oscillator to the first frequency mode, hence the subindex  $v$  and the corresponding summation is dismissed and the resonator Hamiltonian becomes  $\tilde{\mathcal{H}}_n^R = \hbar \omega_n a_n^\dagger a_n$ , in which the zero-point energy is also dropped to simplify.

The interaction Hamiltonian (A22) is also quantized as

$$\mathcal{H}_n^I = \hbar \kappa_n^{\text{cap}} (a_n - a_n^\dagger)(a_{n+1} - a_{n+1}^\dagger) + \hbar \kappa_n^{\text{ind}} (a_n + a_n^\dagger)(a_{n+1} + a_{n+1}^\dagger), \quad (\text{A28})$$

where

$$\kappa_n^{\text{cap}} = 2\chi_c u_n(0) u_{n+1}(0) \sqrt{\omega_n \omega_{n+1}}, \quad (\text{A29})$$

$$\kappa_n^{\text{ind}} = \frac{\chi_{l_n}}{2k_n k_{n+1} L^2} u_n(0) u_{n+1}(0) \sqrt{\omega_n \omega_{n+1}}, \quad (\text{A30})$$

and we have considered just the first mode of the resonators. However, as mentioned before, the coupling between the resonators is weak. Moreover, the resonators are assumed to be similar and in resonance. So we can make the rotating wave approximation (RWA) discarding the ‘‘counter rotating terms’’  $a_n a_{n+1}$  and  $a_n^\dagger a_{n+1}^\dagger$  to obtain

$$\mathcal{H}_n^I = -\hbar \kappa_n(\Phi_{\text{ext}}) (a_n a_{n+1}^\dagger + a_{n+1}^\dagger a_n), \quad (\text{A31})$$

where

$$\kappa_n(\Phi_{\text{ext}}) = -\kappa_n^{\text{ind}}(\Phi_{\text{ext}}) + \kappa_n^{\text{cap}}, \quad (\text{A32})$$

and we have stressed the external field dependency of the couplings by including it in the corresponding arguments. The total Hamiltonian of the system is therefore as in Eq. (1) in the main text, after replacing  $\kappa_n$  with  $\kappa_{nm}$  where  $m = n \pm 1$  [see Fig. 4(a)].

## APPENDIX B: NUMERICAL DATA FOR THE SYSTEM FREQUENCIES

Here we estimate the numerical data for the system parameters.

For a transmission line resonator, an impedance  $Z = \sqrt{l/c} = 50 \Omega$  [20,22,51] may correspond to a capacitance per

unit length  $c = 10^{-10}$  F/m [51] and the impedance per unit length  $l = 2.5 \times 10^{-7}$  H/m. Considering the SQUID junctions capacitance  $C_J = 10^{-15}$  F [52], for a resonator of length  $L = 10^{-2}$  m (comparable with the microwave wavelength), we obtain  $\chi_c = 0.5 \times 10^{-3}$ . On the other hand, the maximum value of  $E_n(\Phi_{\text{ext}})$  in Eq. (A4) is given by  $(4\pi^2/\Phi_0^2)E_J$  which can be calculated using  $E_J = 6.6262 \times 10^{-24}$  J for the Josephson energy [52] and  $\Phi_0 = 2.0679 \times 10^{-15}$  Wb for the flux quantum. Therefore the maximum value of  $\chi_{l_n}$  is obtained as  $|\chi_{l_n}|_{\text{max}} = (4\pi^2/\Phi_0^2)E_J(2Ll) = 0.3059$ .

Actually, the above values for  $\chi_c$  and  $\chi_{l_n}$  have been used in generating the plots in Fig. 5, which give  $k_{n,1}L = 3.0351$  corresponding to the first mode frequency. Supposing all the resonators are identical, or in resonance with the same frequency  $\omega$ , we obtain  $\omega = 607.028$  MHz. The capacitive and inductive couplings in Eqs. (A29) and (A30) are then obtained as  $\kappa^{\text{cap}} = 0.6193$  MHz and  $\kappa^{\text{ind}} = -10.2821$  MHz, respectively, for  $u(0) = A = 1.01$ .

### APPENDIX C: SWITCHING ON AND OFF THE COUPLINGS

Here we infer the magnetic fields pulse profile for switching the couplings.

The time-dependent couplings required for the one-dimensional staggered quantum walk are given in Eq. (5). Such couplings lead to a collection of disjoint pairs of coupled resonators at each time interval  $\tau$ . We can set  $\kappa$  in Eq. (5) to be the maximum value of  $\kappa_n(\Phi_{\text{ext}})$  in Eq. (A32), by setting  $\chi_{l_n} = -|\chi_{l_n}|_{\text{max}}$ , as calculated in the previous section. That corresponds to applying an external magnetic flux equal to the

quantum flux

$$\kappa = \kappa_n(\Phi_{\text{ext}})|_{\Phi_{\text{ext},n}=\Phi_0}, \quad (\text{C1})$$

hence  $\Phi_{\text{on}} = \Phi_0$ .

The required external fluxes for turning off the couplings  $\kappa_{n\pm 1}(\Phi_{\text{ext}})$ , as demanded by Eq. (5), and given by Eq. (A32), are calculated by letting  $\chi_{l_{n\pm 1}} = 4\chi_c(k_n L)^2$  [see Eqs. (A29) and (A30)], where we have assumed that all the resonators are identical. Using such value for  $\chi_{l_{n\pm 1}}$  modifies the resonator frequency  $\omega$  that was calculated in the previous section for the case all the couplings were on. To obtain the new frequency for the case corresponding to a collection of disjoint pairs of coupled resonators, the values for  $\chi_{l_{n-1}}$  and  $\chi_{l_n}$  should be substituted in the transcendental Eq. (A15). Having considered the first mode frequency, we get the system frequencies as  $\omega = 617.8077$  MHz,  $\kappa_n^{\text{ind}} = -10.0054$  MHz,  $\kappa_n^{\text{cap}} = \kappa_{n\pm 1}^{\text{cap}} = 0.6242$  MHz, and  $\kappa_{n\pm 1}^{\text{ind}} = \kappa_{n\pm 1}^{\text{cap}}$ . Moreover, in this case,  $k_n L = 3.089$  which leads to  $\chi_{l_{n\pm 1}} = 0.0191$ , therefore,  $\cos(\pi \Phi_{\text{ext},n}/\Phi_0) = 0.0624$  and we obtain

$$0 = \kappa_{n\pm 1}(\Phi_{\text{ext}})|_{\Phi_{\text{ext},n}=0.4801\Phi_0}, \quad (\text{C2})$$

hence  $\Phi_{\text{off}} = 0.4801\Phi_0$ . When the system topology corresponds to a general triangle-free graph, with degree  $d$ , each resonator is coupled to  $d$  resonators through  $d$  SQUIDs. Therefore, the whole derivation for the 1D array (a triangle-free graph with  $d = 2$ ) is valid here, but slightly modified to include the extra SQUIDs coupled to each resonator. Finally, an isolated pair of coupled resonators can be realized by turning on a specific coupling and turning off the remaining  $d - 1$  ones.

- 
- [1] R. Portugal, *Quantum Walks and Search Algorithms* (Springer, New York, 2013).
- [2] Y. Aharonov, L. Davidovich, and N. Zagury, *Phys. Rev. A* **48**, 1687 (1993).
- [3] E. Farhi and S. Gutmann, *Phys. Rev. A* **58**, 915 (1998).
- [4] J. Lozada-Vera, A. Carrillo, O. P. S. Neto, J. K. Moqadam, M. D. LaHaye, and M. C. Oliveira, *EPJ Quantum Technol.* **3**, 1 (2016).
- [5] A. M. Childs and J. Goldstone, *Phys. Rev. A* **70**, 022314 (2004).
- [6] R. Portugal, *Phys. Rev. A* **93**, 062335 (2016).
- [7] R. Portugal, *Quant. Info. Proc.* **15**, 1387 (2016).
- [8] R. Portugal, R. Santos, T. Fernandes, and D. Gonçalves, *Quant. Info. Proc.* **15**, 85 (2016).
- [9] R. Portugal, S. Boettcher, and S. Falkner, *Phys. Rev. A* **91**, 052319 (2015).
- [10] M. Falk, [arXiv:1303.4127](https://arxiv.org/abs/1303.4127).
- [11] M. Szegedy, in *FOCS '04 Proceedings of the 45th Annual IEEE Symposium on Foundations of Computer Science* (IEEE Computer Society, Washington, DC, 2004), pp. 32–41.
- [12] R. Portugal, M. C. de Oliveira, and J. K. Moqadam, *Phys. Rev. A* **95**, 012328 (2017).
- [13] A. Patel, K. S. Raghunathan, and P. Rungta, *Phys. Rev. A* **71**, 032347 (2005).
- [14] R. Portugal and T. D. Fernandes, [arXiv:1701.01468](https://arxiv.org/abs/1701.01468).
- [15] M. H. Devoret and R. J. Schoelkopf, *Science* **339**, 1169 (2013).
- [16] F. Nori and J. You, *Principles and Methods of Quantum Information Technologies* (Springer, Berlin, 2016), pp. 461–476.
- [17] R. Barends, A. Shabani, L. Lamata, J. Kelly, A. Mezzacapo, U. L. Heras, R. Babbush, A. G. Fowler, B. Campbell, Y. Chen, Z. Chen, B. Chiaro, A. Dunsworth, E. Jeffrey, E. Lucero, A. Megrant, J. Y. Mutus, M. Neeley, C. Neill, P. J. J. O'Malley, C. Quintana, P. Roushan, D. Sank, A. Vainsencher, J. Wenner, T. C. White, E. Solano, H. Neven, and J. M. Martinis, *Nature (London)* **534**, 222 (2016).
- [18] A. A. Houck, H. E. Türeci, and J. Koch, *Nat. Phys.* **8**, 292 (2012).
- [19] I. M. Georgescu, S. Ashhab, and F. Nori, *Rev. Mod. Phys.* **86**, 153 (2014).
- [20] B. Peropadre, D. Zueco, F. Wulschner, F. Deppe, A. Marx, R. Gross, and J. J. García-Ripoll, *Phys. Rev. B* **87**, 134504 (2013).
- [21] A. Baust, E. Hoffmann, M. Haeblerlein, M. J. Schwarz, P. Eder, J. Goetz, F. Wulschner, E. Xie, L. Zhong, F. Quijandria, B. Peropadre, D. Zueco, J.-J. García Ripoll, E. Solano, K. Fedorov, E. P. Menzel, F. Deppe, A. Marx, and R. Gross, *Phys. Rev. B* **91**, 014515 (2015).
- [22] F. Wulschner, J. Goetz, F. Koessel, E. Hoffmann, A. Baust, P. Eder, M. Fischer, M. Haeblerlein, M. Schwarz, M. Pernpeintner *et al.*, *EPJ Quantum Technol.* **3**, 1 (2016).
- [23] S. H. W. van der Ploeg, A. Izmalkov, A. M. van den Brink, U. Hübner, M. Grajcar, E. Il'ichev, H.-G. Meyer, and A. M. Zagoskin, *Phys. Rev. Lett.* **98**, 057004 (2007).



- [24] R. C. Bialczak, M. Ansmann, M. Hofheinz, M. Lenander, E. Lucero, M. Neeley, A. D. O'Connell, D. Sank, H. Wang, M. Weides, J. Wenner, T. Yamamoto, A. N. Cleland, and J. M. Martinis, *Phys. Rev. Lett.* **106**, 060501 (2011).
- [25] Y. Chen, C. Neill, P. Roushan, N. Leung, M. Fang, R. Barends, J. Kelly, B. Campbell, Z. Chen, B. Chiaro, A. Dunsworth, E. Jeffrey, A. Megrant, J. Y. Mutus, P. J. J. O'Malley, C. M. Quintana, D. Sank, A. Vainsencher, J. Wenner, T. C. White, M. R. Geller, A. N. Cleland, and J. M. Martinis, *Phys. Rev. Lett.* **113**, 220502 (2014).
- [26] M. R. Geller, E. Donate, Y. Chen, M. T. Fang, N. Leung, C. Neill, P. Roushan, and J. M. Martinis, *Phys. Rev. A* **92**, 012320 (2015).
- [27] T. Hime, P. A. Reichardt, B. L. T. Plourde, T. L. Robertson, C.-E. Wu, A. V. Ustinov, and J. Clarke, *Science* **314**, 1427 (2006).
- [28] A. O. Niskanen, Y. Nakamura, and J.-S. Tsai, *Phys. Rev. B* **73**, 094506 (2006).
- [29] A. O. Niskanen, K. Harrabi, F. Yoshihara, Y. Nakamura, S. Lloyd, and J. S. Tsai, *Science* **316**, 723 (2007).
- [30] Y. Yin, Y. Chen, D. Sank, P. J. J. O'Malley, T. C. White, R. Barends, J. Kelly, E. Lucero, M. Mariantoni, A. Megrant, C. Neill, A. Vainsencher, J. Wenner, A. N. Korotkov, A. N. Cleland, and J. M. Martinis, *Phys. Rev. Lett.* **110**, 107001 (2013).
- [31] M. Pierre, I.-M. Svensson, S. R. Sathyamoorthy, G. Johansson, and P. Delsing, *Appl. Phys. Lett.* **104**, 232604 (2014).
- [32] I.-C. Hoi, A. F. Kockum, T. Palomaki, T. M. Stace, B. Fan, L. Tornberg, S. R. Sathyamoorthy, G. Johansson, P. Delsing, and C. M. Wilson, *Phys. Rev. Lett.* **111**, 053601 (2013).
- [33] M. S. Allman, J. D. Whittaker, M. Castellanos-Beltran, K. Cicak, F. da Silva, M. P. DeFeo, F. Lecocq, A. Sirois, J. D. Teufel, J. Aumentado, and R. W. Simmonds, *Phys. Rev. Lett.* **112**, 123601 (2014).
- [34] Y. Wu, L.-P. Yang, Y. Zheng, H. Deng, Z. Yan, Y. Zhao, K. Huang, W. J. Munro, K. Nemoto, D.-N. Zheng *et al.*, [arXiv:1605.06747](https://arxiv.org/abs/1605.06747).
- [35] B. V. Correa, A. Kurcz, and J. J. García-Ripoll, *J. Phys. B* **46**, 224024 (2013).
- [36] F. Mei, V. M. Stojanović, I. Siddiqi, and L. Tian, *Phys. Rev. B* **88**, 224502 (2013).
- [37] X. Deng, C. Jia, and C.-C. Chien, *Phys. Rev. B* **91**, 054515 (2015).
- [38] R. Stassi, S. De Liberato, L. Garziano, B. Spagnolo, and S. Savasta, *Phys. Rev. A* **92**, 013830 (2015).
- [39] X.-H. Deng, C.-Y. Lai, and C.-C. Chien, *Phys. Rev. B* **93**, 054116 (2016).
- [40] K. Manouchehri and J. Wang, *Physical Implementation of Quantum Walks* (Springer, Berlin, 2014).
- [41] B. Johnson, M. Reed, A. Houck, D. Schuster, L. S. Bishop, E. Ginossar, J. Gambetta, L. DiCarlo, L. Frunzio, S. Girvin *et al.*, *Nat. Phys.* **6**, 663 (2010).
- [42] M. Hofheinz, E. Weig, M. Ansmann, R. C. Bialczak, E. Lucero, M. Neeley, A. O'Connell, H. Wang, J. M. Martinis, and A. Cleland, *Nature (London)* **454**, 310 (2008).
- [43] M. Hofheinz, H. Wang, M. Ansmann, R. C. Bialczak, E. Lucero, M. Neeley, A. O'Connell, D. Sank, J. Wenner, J. M. Martinis *et al.*, *Nature (London)* **459**, 546 (2009).
- [44] J. Koch, T. M. Yu, J. Gambetta, A. A. Houck, D. I. Schuster, J. Majer, A. Blais, M. H. Devoret, S. M. Girvin, and R. J. Schoelkopf, *Phys. Rev. A* **76**, 042319 (2007).
- [45] The description for even  $N$  must be changed accordingly.
- [46] S. Aaronson and A. Arkhipov, in *Proceedings of the Forty-Third Annual ACM Symposium on Theory of Computing* (ACM, New York, 2011), pp. 333–342.
- [47] B. Peropadre, G. G. Guerreschi, J. Huh, and A. Aspuru-Guzik, *Phys. Rev. Lett.* **117**, 140505 (2016).
- [48] D. M. Pozar, *Microwave Engineering* (John Wiley & Sons, New York, 2005).
- [49] S. M. Girvin, *Lecture Notes of the Les Houches Summer School, Session XCVI, July 2011* (Oxford University Press, Oxford, 2014), Vol. 96, Chap. 3, pp. 113–255.
- [50] K. A. Delin and T. P. Orlando, *Foundations of Applied Superconductivity* (Addison-Wesley, Reading, MA, 1991).
- [51] M. Göppl, A. Fragner, M. Baur, R. Bianchetti, S. Filipp, J. Fink, P. Leek, G. Puebla, L. Steffen, and A. Wallraff, *J. Appl. Phys.* **104**, 113904 (2008).
- [52] J. Koch, A. A. Houck, K. L. Hur, and S. M. Girvin, *Phys. Rev. A* **82**, 043811 (2010).